The Astrophysical Journal, 864:46 (8pp), 2018 September 1 https://doi.org/10.3847/1538-4357/aad2d5

SU Lyn: Diagnosing the Boundary Layer with UV and Hard X-Ray Data

R. Lopes de Oliveira[1,2,3], J. L. Sokoloski[4], G. J. M. Luna[5,6,7], K. Mukai[8,3], and T. Nelson[9]
[1] X-ray Astrophysics Laboratory, NASA Goddard Space Flight Center, Greenbelt, MD 20771, USA; raimundo.lopesdeoliveirafilho@nasa.gov, rlopes@ufs.br
[2] Departamento de Física, Universidade Federal de Sergipe, Av. Marechal Rondon, S/N, 49000-000, São Cristóvão, SE, Brazil
[3] Department of Physics, University of Maryland, Baltimore County, 1000 Hilltop Circle, Baltimore, MD 21250, USA
[4] Columbia Astrophysics Lab 550 W120th St., 1027 Pupin Hall, MC 5247 Columbia University, New York, NY 10027, USA
[5] CONICET-Universidad de Buenos Aires, Instituto de Astronomía y Física del Espacio, (IAFE), Av. Inte. Güiraldes 2620, C1428ZAA, Buenos Aires, Argentina
[6] Universidad de Buenos Aires, Facultad de Ciencias Exactas y Naturales, Buenos Aires, Argentina
[7] Universidad Nacional Arturo Jauretche, Av. Calchaquí 6200, F. Varela, Buenos Aires, Argentina
[8] CRESST and X-ray Astrophysics Laboratory, NASA Goddard Space Flight Center, Greenbelt, MD 20771, USA
[9] Department of Physics and Astronomy, University of Pittsburgh, Pittsburgh, PA 15260, USA
Received 2018 June 8; revised 2018 July 9; accepted 2018 July 9; published 2018 August 29

Abstract

Symbiotic stars in which the symbiotic phenomenon is powered solely by accretion, often at an average rate that is higher than in cataclysmic variable stars, provide an important opportunity to diagnose boundary layers around disk-accreting white dwarfs. Here, we investigate SU Lyncis (SU Lyn), a recently discovered example of a purely accretion-powered symbiotic star, using the first reliable X-ray spectroscopy, obtained with *NuSTAR*, and ultraviolet (UV) photometry obtained with *Swift*. SU Lyn has hard, thermal, X-ray emission that is strongly affected by a variable local absorber that has little impact on the UV emission. Its X-ray spectrum is described well using a plasma cooling from $kT \approx 21$ keV, with a 3–30 keV luminosity of approximately 4.9×10^{32} erg s^{-1}. The spectrum is also consistent with the presence of reflection with an amplitude of 1.0, although in that case, the best-fit plasma temperature is 20%–25% lower. The UV to X-ray luminosity ratio of SU Lyn changed significantly between 2015 and 2016. We interpret this as a consequence of a drop by almost 90% in the accretion rate. Whereas the UV luminosity of the disk responded linearly, the luminosity of the optically thin (hard X-ray) emission from the boundary layer remained roughly constant because the boundary layer changed from partially optically thick to almost completely optically thin. Under this interpretation, we place a lower limit on the white dwarf mass of $0.7\,M_{\odot}$ ($0.8\,M_{\odot}$ if we neglect reflection).

Key words: binaries: symbiotic – stars: individual (SU Lyncis) – ultraviolet: stars – X-rays: binaries

1. Introduction

Phenomenologically, symbiotic stellar binaries were initially defined by the presence of strong high-excitation emission lines in the optical on top of a red giant continuum (Kenyon 1986). They are associated with binary systems involving a red giant star and an accretor that might be a white dwarf or a neutron star (see Mukai 2017 for a review). Most members of the class have been discovered in the optical using the strong high-excitation lines as the defining characteristic.

What may be just the tip of an iceberg came from the discovery by Mukai et al. (2016) that the red giant SU Lyncis (SU Lyn) is the optical counterpart of a hard, thermal X-ray source. Its properties, including excess in ultraviolet (UV) when compared with non-interacting red giants and variability in optical lines of Hydrogen Balmer series, [Ne III], and Ca II, are consistent with accretion onto a white dwarf without shell burning. The hard X-ray nature of the system was first identified by the authors from the *Swift*/BAT hard X-ray all-sky survey, then followed by a coordinated follow up in X-rays and UV conducted with the *Swift* satellite (X-Ray Telescope (XRT) and UltraViolet and Optical Telescope (UVOT) cameras) and in the optical through medium- and high-resolution spectroscopy from two telescopes at Asiago. Altogether, the observations supported that the X-ray emission is dominated by an optically thin plasma that can be as hot as 2×10^8 K (kT of about 17 keV, from the APEC model) or peaking at 3×10^8 K when assuming a cooling-flow model (MKCFLOW). These properties are reminiscent of the δ-type symbiotic stars, which is currently composed of about a dozen members and as defined by Luna et al. (2013): "highly absorbed, hard X-ray sources [...]. The likely origin is the boundary layer between an accretion disk and the white dwarf." SU Lyn is a long-term variable X-ray emitter in both soft and hard X-rays, strongly affected by local absorbers that change with time. Besides revealing the presence of weak high-ionization lines, the optical observations led Mukai et al. (2016) to conclude that SU Lyn is an M5.8III cool giant star located at $d = 640 \pm 100$ pc, and finally pointing out that it is a member of a symbiotic system.

The potential significance of this discovery lies in the fact that there may be a large population of symbiotic stars with weak emission lines. Because of this, this population has remained hidden, only to be revealed by their high energy emission. The number of symbiotic stars in the Galaxy and their contribution to the integrated X-ray emission have likely been underestimated. Moreover, this new subclass of symbiotic stars opens up a new avenue in which to investigate accretion, and the evolution of symbiotic stars. The prototype, SU Lyn, is likely to be among the brightest member of the subclass, and therefore deserves further attention. In this paper, we present a more in depth investigation of SU Lyn in the X-ray and UV domains using coordinated *NuSTAR* and *Swift* observations.

2. Observations

While Mukai et al. (2016) investigated the hard X-ray properties of SU Lyn using *Swift*/BAT data, the sensitivity of this instrument is such that it takes months of integration to securely detect this source (Mukai et al. used 120 day bins in

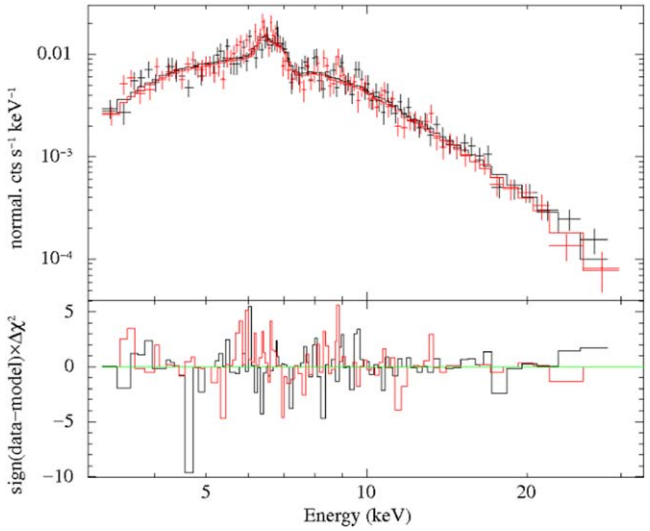

Figure 1. *NuSTAR* X-ray spectra: FPMA in black and FPMB in red. Spectral fit corresponds to model 1 (M1; TBABS*(APEC+GAUSS)).

their Figure 1, showing the BAT light curve). The best signal-to-noise ratio (S/N), integrated over the high state in the 15–35 keV range, is 16.3. As we must divide these data into multiple energy bins for spectral analysis, hard X-ray spectral parameters of SU Lyn cannot be tightly constrained using *Swift*/BAT.

We therefore observed SU Lyn with the *Nuclear Spectroscopic Telescope Array* (*NuSTAR*; Harrison et al. 2013) mission. The total exposure time of about 40.9 ks, for both focal plane modules A and B (FPMA and FPMB, respectively), was spread over approximately 80 ks on 2016 August 12–13 (ObsID 30201025002; Table 1). During about 9.4 ks out of that time, we also observed it using the Neil Gehrels Swift Observatory (Gehrels et al. 2004) using both XRT and UVOT instruments (ObsID 00081892001). We added to our analysis the *Swift*/UVOT (ObsID 00034150001, taken on 2015 November 20) and BAT data of SU Lyn investigated by Mukai et al. (2016) to perform a comparative study of the state of the source in UV and X-rays.

We used the XRT in photon counting mode because the expected X-ray flux was modest. However, the CCD detector for the XRT is also sensitive to optical and near-infrared photons, and lead to a phenomenon called optical loading.[10] When numerous optical/near-IR photons land on the same pixel during a single CCD exposure, the total amount of charge resulting from this can resemble that from a single, soft X-ray photon. This can result in spurious events at soft energies. Such a soft component is seen in the 2016 August XRT data on SU Lyn.

In addition, the onboard software uses the distribution of charges across neighboring pixels to distinguish between X-ray events and particle hits. True X-ray photons lead to a tightly clustered set of charges (single pixel to a 2 × 2 square), while particle hits tend to leave charges in multiple adjacent pixels. In the presence of optical loading, X-ray photons can be misinterpreted as having particle hit-like distribution of charges, and therefore be rejected in standard screening. During both 2015 and 2016 observations of SU Lyn, while the events in the unscreened files have a point-spread function like spatial distribution, the cleaned files have a more diffuse appearance with a central hole. We conclude that optical loading led to the loss of true X-ray event, and distortion of pulse height distribution of X-ray events that survive the screening. We therefore did not use the XRT data in this paper, and also conclude that the X-ray spectral parameters of SU Lyn derived from *Swift*/XRT data by Mukai et al. (2016) are unreliable, thereby making the *NuSTAR* data the first reliable X-ray spectra of SU Lyn.

[10] http://www.swift.ac.uk/analysis/xrt/optical_loading.php

Table 1
2016 August Observations of SU Lyn

	NuSTAR	*Swift*
ObsID	30201025002	00081892001
Start time	2016 Aug 12 20:16:08	2016 Aug 12 22:28:58
Stop time	2016 Aug 13 17:36:08	2016 Aug 13 10:41:52
Exposure	40,920 s	9411 s

Data reduction and analysis were carried out with HEASOFT version 6.22 using the specific tools for each mission and calibration files available in 2017 August and December for the *NuSTAR* and *Swift* data, respectively. For the *NuSTAR* data, we applied the NUPIPELINE and then the NUPRODUCTS to obtain science products, while for the *Swift*/UVOT data we used the tasks COORDINATOR, UVOTSCREEN, XSELECT, and UVOTEVTLC. The typical absolute astrometric uncertainty of the *NuSTAR* is ±8″, with a usual relative offset of 5″–10″ for one *NuSTAR* module with respect to the other—drifting on time depending essentially on the thermal condition and therefore on the illumination of *NuSTAR* by the Sun (B. Grefenstette 2018, private communication). Thus, we use different extraction regions for FPMA and FMPB based on their individual images.

The spectral analysis was conducted with the X-ray spectral fitting package XSPEC V12.9.1M. It was based on simultaneous fits of *NuSTAR* FPMA and FPMB data from the minimum detector threshold of 3 keV (Madsen et al. 2015 and references therein) to 30 keV, because background dominates at higher energies. The energy binning was set to have a minimum of 25 counts in each bin. A multiplicative constant was applied for each data set in XSPEC to account for possible cross-calibration uncertainties but the difference is limited to 5%. The BAT data set was important to characterize the photometric variability of the system. All errors and comparisons discussed in this work are at a 1σ confidence level.

3. Results

3.1. X-Ray Spectral Energy Distribution

We constructed two spectra from the whole *NuSTAR* observation, one from the FPMA and another from the FPMB data, then fitted simultaneously with XSPEC (Figure 1). Their shape and the clear presence of emission lines of the Fe K complex around 6.7 keV reinforces three characteristics previously reported by Mukai et al. (2016) that are investigated in detail in this work: hard, thermal, and locally absorbed X-ray emission.

We adopt the TBABS model to account for the photoelectric absorption (Wilms et al. 2000). Two models based on thermal plasma emission were individually applied to test two different hypotheses: the emission from a single-temperature plasma component (APEC) and the emission from a cooling-flow plasma (MKCFLOW). The abundance table applied in the

models is that of Wilms et al. (2000). For comparison, we find that the use of such a table results in mutually consistent temperatures (kTs) but absorption columns (in equivalent Hydrogen column, $N_{\rm H}$) and abundances that are systematically higher by 52% and 75%, respectively, with respect to the values obtained from solar abundance vector set to Anders & Grevesse (1989). In all cases, we added a Gaussian line (GAUSSIAN) to account for the excess due to the fluorescence Fe line at 6.4 keV. As the line parameters are not well determined during the fit, the centroid was fixed at the rest energy value and the line width (σ) was fixed to 1 eV, while the normalization was a free parameter during the fit.

Single-temperature plasma and cooling-flow spectral models both provided acceptable fits to the *NuSTAR* spectra. We first attempted to fit the spectra with the simplest model, TBABS*(APEC+GAUSS) (M1). We found that the spectrum of SU Lyn is well described by a plasma with temperature (kT) of $12.0^{+0.8}_{-0.7}$ keV and abundance (Z) of $0.90^{+0.22}_{-0.19}$ relative to solar values ($Z_{\odot}$). The photoelectric absorption is equivalent to a Hydrogen column ($N_{\rm H}$) of $19.8^{+1.8}_{-1.8} \times 10^{22}$ cm^{-2}. The ionized lines of the Fe K complex are well described by M1. This fit results in χ^2_{ν} equal to 1.09 for 182 degrees of freedom (d.o.f).

The other model, TBABS*(MKCFLOW+GAUSS) (M2), did not significantly improve the fit. M2 resulted in $N_{\rm H} = 23.3^{+2.1}_{-2.3} \times 10^{22}$ cm^{-2} and $Z = 0.75^{+0.20}_{-0.16}$ $Z_{\odot}$. As the low energies are not covered by the *NuSTAR* spectra, we fixed the low temperature component of the MKCFLOW to its lower limit of $kT = 80.8$ eV. The maximum temperature parameter of this model has $kT_{\rm H} = 21.1^{+2.6}_{-1.9}$ keV. The χ^2_{ν} obtained from M2 is 1.07 for 182 d.o.f. For M2 we set the *switch* parameter to 2, such that the MKCFLOW model, originally based on the MEKAL code, was calculated by running the APEC (AtomDB) table. We adopt a redshift of 1.49×10^{-7} for the MKCFLOW component of M2 and the default cosmology parameters in XSPEC ($H_0 = 70$ $q_0 = 0$, and $\Lambda_0 = 0.73$) to take into account the distance of the system, which Mukai et al. (2016) estimated to be 640 pc (consistent with the *Gaia* DR2 parallax of 1.493 ± 0.096 mas; Gaia Collaboration et al. 2016, 2018). We tested the inclusion of a partial covering fraction absorption (PCFABS), which is sometimes present in other symbiotic systems, but the fit was not improved. Table 2 summarizes the spectral parameters from the models cited above.

Table 2
Best-fit Spectral Parameters from the *NuSTAR* Observation

Parameter	APEC	
$N_{\rm H}$ (10^{22} cm^{-2})	$19.8^{+1.8}_{-1.8}$	$18.3^{+2.2}_{-2.3}$
kT (keV)	$12.0^{+0.8}_{-0.7}$	$9.9^{+1.1}_{-0.8}$
Z ($Z_{\odot}$)	$0.90^{+0.22}_{-0.19}$	$0.72^{+0.17}_{-0.14}$
rel$_{\rm refl}$	...	$1.0^{+0.8}_{-0.6}$
χ^2_{ν}/d.o.f.	1.09/182	1.08/181
$F_{(3-30{\rm keV})}$[a]	9.6 ± 0.8	9.3 ± 1.0
	MKCFLOW	
$N_{\rm H}$ (10^{22} cm^{-2})	$23.3^{+2.1}_{-2.3}$	$22.5^{+2.4}_{-3.0}$
$kT_{\rm high}$ (keV)	$21.1^{+2.6}_{-1.9}$	$16.3^{+4.2}_{-2.7}$
$kT_{\rm low}$ (keV)	0.0808	0.0808
Z ($Z_{\odot}$)	$0.75^{+0.20}_{-0.16}$	$0.59^{+0.19}_{-0.14}$
rel$_{\rm refl}$	...	$0.9^{+1.5}_{-0.8}$
χ^2_{ν}/d.o.f.	1.07/182	1.07/181
$F_{(3-30{\rm keV})}$[a]	10.0 ± 1.3	9.9 ± 1.1

Note. The models are M1 [TBABS*(APEC+GAUSS)] and M2 [TBABS*(MKCFLOW+GAUSS)], in the second column, and the same but with the thermal component convolved with a REFLECT component in the third column.
[a] Fluxes are unabsorbed and in units of 10^{-12} erg cm^{-2} s^{-1}.

3.2. Reflection and Consequences for the Derived Plasma Properties

Although the inclusion of the REFLECTION component does not improve the χ^2_{ν} goodness of the fit with respect to "pure" models, our spectral fitting indicates that this component could be present in SU Lyn. We used the REFLECT model in XSPEC in order to check for the presence of a Compton hump that could be due to "reflection" of intrinsic X-rays over the white dwarf or nearby cold material. This component was convolved by the thermal components in M1 and M2. We assumed that the abundance of the REFLECT component, including the iron abundance, was equal to the abundance of the corresponding thermal component and allowed them to vary while linked during the fit.

Allowing the reflection scaling factor to vary during the fitting resulted in values equal to $0.98^{+0.84}_{-0.58}$ and $0.87^{+1.46}_{-0.77}$ from M1 and M2, respectively. The inclination angle i between the normal to the reflector and the line of sight (Magdziarz & Zdziarski 1995) was not constrained in the fit, so we set it such that $\cos(i) = 0.45$. With the inclusion of reflection, the best-fit kT value is lower than in the fit without reflection. Although the 1σ error ranges overlap, the best-fit temperature without reflection (21.1 keV) is outside the range obtained with reflection (13.6–20.5 keV), and vice versa (16.3 keV and 19.2–23.7 keV; see Table 2). In general, when the statistical quality of the data is higher, the drop in kT with the addition of a reflection component is statistically significant (as was the case with RT Cru; Luna et al. 2018). Therefore, we advise caution when the white dwarf mass is derived exclusively using fits without reflection. In this work, we present analyses with and without reflection.

The spectrum of SU Lyn is marked by a noticeable excess due to the fluorescent and ionized lines of the Fe K complex. We inferred a line intensity of $(1.8 \pm 0.3) \times 10^{-5}$ photons cm^{-2} s^{-1} and equivalent width (EW) of 150–380 eV for the fluorescent Fe line at 6.4 keV. The measured EW does not allow us to distinguish the cases with or without reflection because its lower limit is still consistent with the contribution being only due to the local X-ray absorber (see Figure 7 of Ezuka & Ishida 1999), while the higher end of allowed values would appear to require the contribution from both the absorber and reflection.

3.3. Photometric and Spectral Variability

3.3.1. X-Ray Photometric Variability

SU Lyn is a variable X-ray/UV source, and therefore caution is required when investigating properties from spectra that accumulate information acquired over long timescales because the long-term variability is energy dependent. However, following the expectation that the plasma temperature—which strongly depends on the gravitational potential well promoted by the WD—is not variable, and that the absorption has little effect in hard X-rays, we compare the *NuSTAR* spectrum with the BAT averaged spectrum constructed by co-adding observations from 2004 December 8 to 2016 January 11, which is the average of "normal state" and "high state" (Mukai

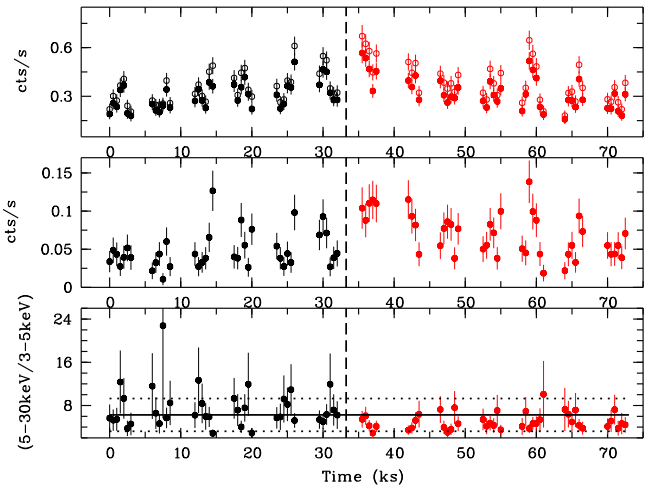

Figure 2. *NuSTAR* X-ray light curves and hardness ratio (FPMA+FPMB). Top: 3–30 keV (open circles) and 5–30 keV (filled circles). Middle: 3–5 keV. Bottom: (5–30 keV)/(3–5 keV). The vertical line delimits the first (black) and second (red) halves of the observation explored in Figure 4. The horizontal lines in the bottom panel represent the mean value (solid line) and the corresponding limits at 1σ. The t_0 corresponds to 2016 August 12 at 20:25:00.200 UTC, the start time of the *NuSTAR* exposures. Time bin size is 500 s.

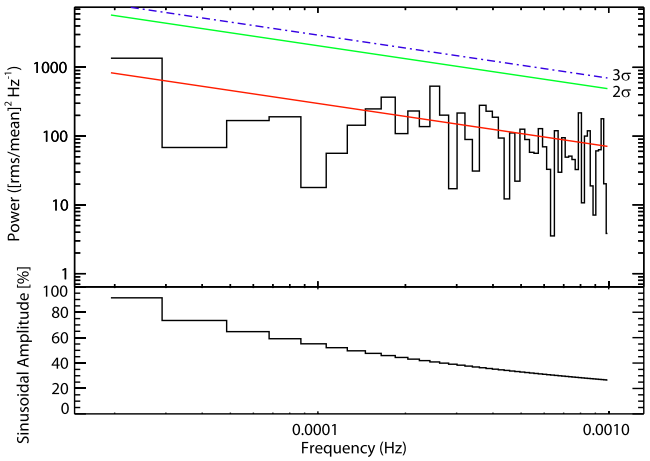

Figure 3. *NuSTAR* power spectrum from the 3 to 30 keV FPMA+FPMB light curve with bins of 500 s. The power-law model for the red noise is shown in solid (red) line and 2σ (green) and 3σ (blue) upper limits on the expected power are shown in dotted–dashed curves. Bottom: upper limit (3σ) on the sinusoidal fractional amplitude as a function of frequency.

et al. 2016). Both can be described by the same model being the only noticeable difference associated to the flux that drops during the *NuSTAR* observation (Section 3.3.1). The corresponding mean flux from the averaged BAT spectrum was obtained by integrating the absorbed APEC model (M1) in a simultaneous fit of the *NuSTAR* and BAT spectra.

Although the average BAT spectrum still had a low S/N, this exercise showed that the *NuSTAR* flux at the 15–35 keV energy range in 2016 August (of about 2.5×10^{-12} erg cm^{-2} s^{-1}) was about 47% of the flux derived from the BAT observations between 2004 and 2016 (of about 5.3×10^{-12} erg cm^{-2} s^{-1}). Repeating the exercise with the BAT spectrum corresponding to the time interval associated to the high state of SU Lyn described by Mukai et al. (2016), we found that the 15–35 keV flux during the *NuSTAR* observations in 2016 August corresponds to ≈14% of the high state observed with *Swift*/BAT between 2010 October 14 and 2012 August 1 (≈1.8×10^{-11} erg cm^{-2} s^{-1}). In both cases, using the "averaged" or "high state" BAT spectrum in the simultaneous fit with the *NuSTAR* spectra, the values obtained for the absorption column, temperature, and abundance are fully consistent with those presented in Table 2. As presented by Mukai et al. (2016), the normal state before and after the high state was about 1/2 of the "averaged" flux, hence SU Lyn in 2016 August appears to have been at a similar hard X-ray luminosity level as the normal state.

Variability on a shorter timescale (>100 s) was accessible from the *NuSTAR* observation. Figure 2 presents the light curve in the widest possible energy range (3–30 keV; open circles in the top panel). It also includes two other light curves from the hardest (5–30 keV; top panel) and softest (3–5 keV; middle panel) photons and the corresponding hardness ratio (hard/soft; bottom panel). All light curves were constructed by combining the FPMA and FPMB data in time bins of 500 s. Both soft and hard light curves are marked by variations up to a factor 2.5 on timescales as short as 500 s. There is marginal evidence from the photometry that SU Lyn exhibits spectral evolution with time, especially when comparing the first and second halves of the observation. Figure 2 (bottom) suggests that the hardness ratio is more variable and on average higher during the first half, indicating a higher fraction of hard X-rays or lower fraction of soft X-rays in comparison with the rest of the observation. While the suspicion of fast variability (of about 500 s) cannot be accessed, with the flux being consistent with the mean value at a 1σ level even from the photometry (horizontal lines at the bottom of Figure 2), the variability in 10 hr can be investigated from spectroscopy. We return to latter point in the Section 3.3.3.

3.3.2. Search for Period Modulation in X-Rays

We searched for periodic modulation in X-rays by investigating the Fourier power spectrum of the 3–30 keV *NuSTAR* (FPMA+FPMB) light curve binned in 500 s. A simple power-law model was applied to describe the log-log power spectrum from 10^{-5} to 10^{-3} Hz and a deviation at a 3σ level was obtained by following the method outlined by Vaughan (2005). Also, the upper limits on the sinusoidal fractional amplitude as a function of frequency were calculated following Equation (13) in Israel & Stella (1996). Because no peak exceeds a 3σ detection threshold, there is no evidence for periodic modulation from the *NuSTAR* data (Figure 3).

3.3.3. Evaluating X-Ray Spectral Evolution

Figure 2 (bottom) suggests that the X-ray hardness ratio of SU Lyn was on average higher during the first half of the observation. To evaluate this suspicion, we split the observation into two segments and performed spectral analysis on each segment separately, with a pair of FPMA and FPMB spectra from the first six orbits and another pair from the rest (seven orbits). The vertical line in Figure 2 shows where we split the data and Figure 4 shows the corresponding unfolded spectra (only FPMA, for clarity), with both following the same color code.

We consider two cases using M2 (both without reflection). In the first one, the plasma parameters were frozen to those presented in Table 2 ($kT = 21.1$ keV and $Z = 0.75\,Z_\odot$). It resulted in $N_{\rm H} = 28.4^{+2.2}_{-2.1} \times 10^{22}$ cm^{-2} for the first half and

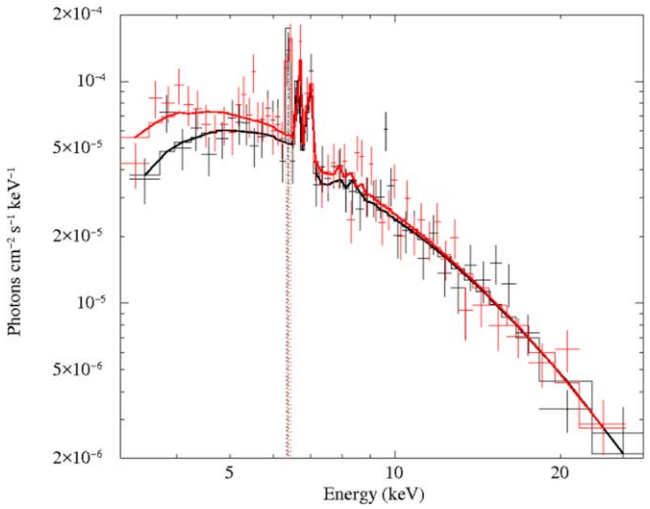

Figure 4. *NuSTAR* unfolded FPMA spectra: black, first half; red, second half (as presented in Figure 2 with the same color code).

$N_{\rm H} = 20.6^{+1.6}_{-1.5} \times 10^{22}\,{\rm cm}^{-2}$ for the second half of the observation (χ^2_ν/d.o.f = 1.07/89 and χ^2_ν/d.o.f = 1.16/111, respectively). Then we considered a second case in which the temperature was free during the fit, resulting in $N_{\rm H} = 28.4^{+3.0}_{-3.0} \times 10^{22}\,{\rm cm}^{-2}$ and $kT = 21.1^{+3.0}_{-2.2}$ keV with χ^2_ν/d.o.f = 1.08/88 for the first half, and $N_{\rm H} = 22.1^{+2.3}_{-2.2} \times 10^{22}\,{\rm cm}^{-2}$ and $kT = 19.2^{+2.0}_{-1.8}$ keV with χ^2_ν/d.o.f = 1.16/110 for the second one.

This analysis reveals a significant decrease in the local absorption by about 25% on a timescale of ∼10 hr, while the properties of the X-ray emitting plasma remained essentially the same, including the unabsorbed flux. Similar results are obtained with M1. The impact of the absorption on the continuum can be seen up to 5 keV (Figure 4 shows the unfolded spectra for the first case cited above, with parameters frozen).

3.3.4. UV Photometric Variability

We compared the recent data set with that collected five months earlier also with the UVM2 filter, and reported by Mukai et al. (2016). Following the procedure adopted by those authors, we use HD 237533 as a comparison star. Figure 5 shows the UV light curves of both SU Lyn and HD 237533. While the count rate of the comparison star remained essentially constant during both campaigns (66.40 ± 3.40 counts s^{-1} and 68.62 ± 4.64 counts s^{-1} for the whole first and second observations, respectively), the brightness of SU Lyn had decreased by a factor of about 8.7 when comparing the mean value registered during the last orbit on 2015 November 20 (137.51 ± 13.34 counts s^{-1}) and that from the orbits on 2016 August 12/13 (15.84 ± 1.85 counts s^{-1}).

Individually, the mean count rates for each orbit of the 2016 observation are consistent at a 1σ level with the mean value from the whole light curve. This is also true when dividing the UVOT data into two portions (see the vertical line in Figure 5, which marks the same time as the vertical line in Figure 2), with the first portion having been conducted during the first half of the *NuSTAR* observation and the second portion carried out during the second half of the *NuSTAR* observation explored in Section 3.3.3. The first portion corresponds to five *Swift* orbits, with a mean count rate of 15.86 ± 2.04 counts s^{-1}, while the second portion was covered by three orbits, from which the mean count rate was 15.58 ± 1.90 counts s^{-1}. Thus, contrary to X-rays, the first and second portions of the observation in UV remained essentially the same and were consistent with the mean value for the whole light curve, even with the 25% drop in the $N_{\rm H}$ affecting the X-rays. However, a difference of about 20% in count rate can be present from one orbit to another, as seen between the second (17.09 ± 1.28 counts s^{-1}) and third (13.49 ± 1.33 counts s^{-1}) orbits.

The fractional rms level of SU Lyn in the *Swift*/UVOT campaign on 2016 remained essentially constant from one orbit to another, ranging from 7.5% to 9.8%, and about 12% for the whole UV light curve. This is consistent with the values pointed out by Mukai et al. (2016) for the UVOT campaign carried out in 2015 November.

4. Discussion

SU Lyn is marked by a hard thermal X-ray emission of moderate luminosity, which is affected by strong and variable local absorption. Both X-ray and UV fluxes vary on short and long timescales. In the following, we discuss the properties of the system as inferred from *NuSTAR* X-ray spectroscopy and in the light of a dramatic decrease in the $L_{\rm UV}/L_{\rm X}$ ratio observed over the course of nine months.

4.1. From the X-Ray Spectroscopy of SU Lyn

Our analysis showed that both single-temperature (APEC) and cooling plasma (MKCFLOW) models describe well the X-ray spectrum of SU Lyn (Table 2). However, a single-temperature plasma model is unphysical: thermal emission cools the plasma, for one thing, and a thermal plasma cannot settle onto the white dwarf until it cools to the photospheric temperature, for another. Such a cooling flow is exactly the situation that the MKCFLOW model represents, with some simplifying assumptions, meaning that this is a more realistic physical model of the X-ray emission from SU Lyn (see Mukai 2017) for a more complete discussion). Moreover, direct evidence for a multi-temperature plasma in another symbiotic star with δ-type X-ray emission was provided by the *Chandra* observation of V658 Car (Eze et al. 2010). While a cooling flow can be associated with either an accretion column or a boundary layer in an accretion disk, the lack of periodic X-ray modulations disfavors magnetic accretion and argues in favor of accretion through a boundary layer.

The cooling-flow model reveals a maximum temperature kT approximately equal to 21 keV, or 16 keV if reflection of hard X-rays in cold material is present. The data are consistent with either models with or without reflection, as judged by the continuum shape (i.e., whether a Compton reflection hump is present) and by the strength of the fluorescent 6.4 keV line. With or without reflection, the unabsorbed flux implies a luminosity of 4.9×10^{32} erg s^{-1} at the 3–30 keV energy band, assuming a distance of 640 pc. Extrapolating the *NuSTAR* response to 0.1–100 keV, we estimate the bolometric luminosity to be 7.4×10^{32} erg s^{-1} and 9.8×10^{32} erg s^{-1} for APEC and MKCFLOW based models, respectively.

The maximum temperature in the boundary layer suggests that the mass of the white dwarf is at least about 0.8 $M_\odot$. In non-magnetic accreting systems in which an accretion disk is formed, approximately half of the potential energy of the falling matter is radiated away in the disk where the Keplerian

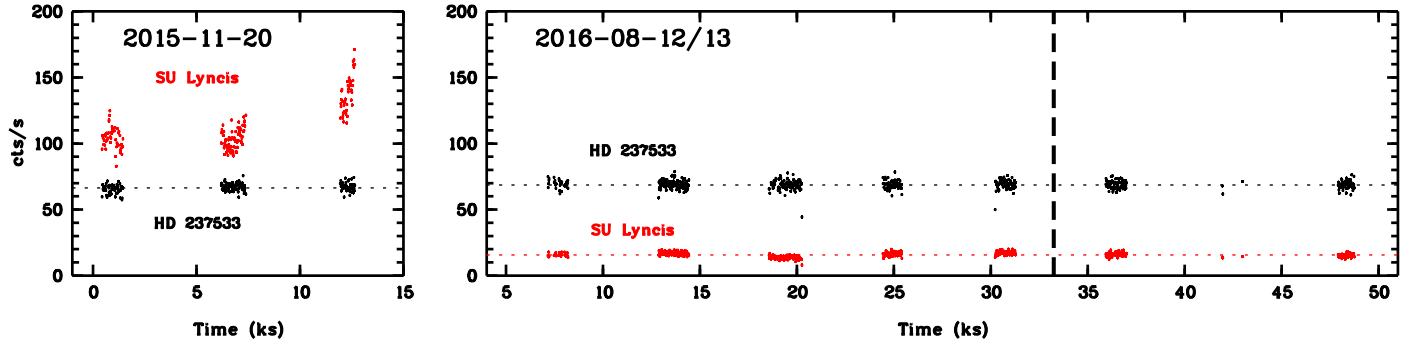

Figure 5. UV light curve (*Swift*/UVOT; UVM2 filter, centered at 2246 Å). The t_0 for the first *Swift*/UVOT exposure (left panel) corresponds to its start time (2015 November 20 at 17:43:48.548 UTC), while the t_0 for the second *Swift* observation (right panel) corresponds to the start time of the *NuSTAR* exposures (2016 August 12 at 20:25:00.200 UTC) for direct comparison with Figure 2. The vertical line in the right panel flags the time used to split the *NuSTAR* observation into two parts (as in Figure 2). Time bin size is 15 s.

velocity corresponds to $(1/2)^2$ times free-fall velocity. Assuming that this is the modus operandi for SU Lyn, the maximum shock temperature ($T_{s,\max}$) comes from the X-ray spectral fits using the MKCFLOW model (M2 in Section 3.1) and allows us to estimate the white dwarf mass ($M_{\rm WD}$). Doing this, we calculate half of the total energy from free-fall from infinity following Frank et al. (2002), assuming the mass–radius relation for white dwarfs suggested by Pringle & Webbink (1975). Factors such as rapid rotation, high core temperature, and high envelope temperature can all modify the mass–radius relationship in principle. However, they all go in the direction of larger radii, and hence the lower limits we derive below on the white dwarf mass and the mass accretion rate are secure. This theoretical approach was successfully applied by Byckling et al. (2010) to explain the locus occupied by a sample of dwarf novae in the $M_{\rm WD}$ versus $T_{s,\max}$ diagram. Our results indicate that the mass of the white dwarf in SU Lyn is consistent with $0.87^{+0.05}_{-0.04}\,M_\odot$ for $T_{s,\max} = 21.1^{+2.6}_{-1.9}$ keV (from the MKCFLOW model), and can be 14% less, $0.76^{+0.10}_{-0.07}\,M_\odot$ if reflection is present (Section 3.2). From this model, the mass accretion through the optically thin portion of the boundary layer is approximately equal to $(1.8 \pm 0.3) \times 10^{-10}\,M_\odot\,{\rm yr}^{-1}$, or $(2.0 \pm 0.2) \times 10^{-10}\,M_\odot\,{\rm yr}^{-1}$ if reflection is present. When the UV luminosity exceeds the X-ray luminosity, part of the boundary layer is likely optically thick, and therefore the values above correspond to lower limits for the mass accretion rate.

4.2. From the Spectral and Photometric Variability

Our observations show that in 2016 the UV emission from SU Lyn had dropped after the high state in 2015 reported by Mukai et al. (2016). These authors reported from *Swift*/UVOT and *GALEX* data that SU Lyn is variable in UV on timescales as short as tens of seconds with a fractional variability of 7%–10%. They reported from *GALEX* data that SU Lyn was much fainter in UV on 2006 December 21 and 2007 January 27 than *Swift*/UVOT showed it to be on 2015 November 20. In the *Swift*/UVOT data, Mukai et al. (2016) also observed that the UVM2 count rate increased by about 30% within 95 minutes from the second to the third and last orbit of the campaign on 2015 November 20 (Figure 5, left).

We show here that SU Lyn underwent a dramatic decrease by a factor 8.7 in the UV flux on an unknown timescale but which is constrained to be less than nine months, the elapsed time between the two recent *Swift*/UVOT observations (2016 August 12 and 2015 November 20; Figure 5). The low state lasted for at least 11.6 hr. We refer to this behavior as "long-term variability," if not for the timescale on which it occurred, then for the duration of the states. It corresponds to a change from $(1.16 \pm 0.11) \times 10^{-13}\,{\rm erg\,s^{-1}\,cm^{-2}\,\AA^{-1}}$, to $(1.34 \pm 0.16) \times 10^{-14}\,{\rm erg\,s^{-1}\,cm^{-2}\,\AA^{-1}}$, in the spectral range covered by the UVM2 filter, and therefore to a drop in the total UV at 2000–4000 Å from $2.3 \times 10^{-10}\,{\rm erg\,s^{-1}\,cm^{-2}}$ to $2.7 \times 10^{-11}\,{\rm erg\,s^{-1}\,cm^{-2}}$. In terms of luminosity, these values correspond to $1.1 \times 10^{34}(d/640\,{\rm pc})^2\,{\rm erg\,s^{-1}}$ and $1.3 \times 10^{33}(d/640\,{\rm pc})^2\,{\rm erg\,s^{-1}}$, respectively. In contrast, the hard X-ray flux observed with *NuSTAR* in 2016 in the 15–35 keV energy band is similar to that seen with *Swift*/BAT during the normal state, as defined by Mukai et al. (2016).

The intervening column affecting X-rays changed significantly from 28×10^{22} to $21 \times 10^{22}\,{\rm cm^{-2}}$ in the course of the *NuSTAR* observation (Section 3.3.3), proving that changes may happen on timescales as short as 10 ks. It suggests that the spikes in the hardness ratio (Figure 2; bottom) are associated with a decrease of softest X-rays (3–5 keV) caused by an increase of the photoelectric absorption that, on average, results in a higher column for the first half than that for the second half of the observation. In this case, the "instantaneous" absorption in the short period of time associated with the "hardness spikes" may be even higher than the inferred value. What could be causing this variation? Despite the complexity in the absorption with time, the X-ray spectrum (3–30 keV) is well described for a simple absorption component. Although this can only be confirmed by sensitive observations including softest X-rays, the results suggest that the intervening material may be inhomogeneous but relatively well distributed over the X-ray emitting sites.

As for SU Lyn, there is also evidence that X-rays of δ-type symbiotics as a whole suffer the effect of local absorbers that are variable on a day to day timescales. Regardless of whether this is due to spatial inhomogeneities or temporal changes, the timescale of the $N_{\rm H}$ variability can be used to constrain the origin of the absorber. In particular, it is unlikely to be the wind of the mass donor: the binary likely has a scale of $\sim$ au, and the wind of a red giant has a characteristic velocity of order $10\,{\rm km\,s^{-1}}$, so it would be difficult for this to lead to variable $N_{\rm H}$ on timescales much shorter than $1\,{\rm au}/10\,{\rm km\,s^{-1}} \approx 6$ months. An origin much closer to the white dwarf is indicated.

The local X-ray absorber does not appear to absorb the UV emission from SU Lyn, as evidenced by the lack of detectable changes in UV count rates between the first and second halves of the *NuSTAR* observation, when the local X-ray absorber

varied significantly. We can understand this in the context of localized absorbers in two possible ways. If the absorber is extremely localized, right next to the X-ray emission region (presumably the boundary layer between the disk and the white dwarf), then it might not obstruct our view of the UV emission region (parts of the Keplerian accretion disk proper). Alternatively, the X-ray absorber might cover both the X-ray and UV emitting regions but may be transparent to UV. This is possible because UV absorption in the ISM is due to dust and molecules, while that in interacting binaries may be due to 10,000 K material ("Fe II Curtain;" Horne et al. 1994) and the localized absorber in SU Lyn may well be too hot for either.

4.3. The Scenario

Whereas the Keplerian part of the accretion disk accounts for the UV radiation, the boundary layer accounts for the X-rays. Mukai et al. (2016) suspected that the boundary layer during the *Swift* observation on 2015 November 20 was at least partially optically thick to X-rays—implying that the WD mass estimate they obtained from X-rays, $1\,M_{\odot}$, is a lower limit. Changes in the ratio of $L_{\rm UV}$ to $L_{\rm X}$ give us clues about the physical conditions in the boundary layer. Assuming that the observed UV is not subject to strong intrinsic absorption, as is the case for the X-ray photons in the 15–35 keV energy regime, we use the $L_{\rm UV}/L_{\rm X;15-35keV}$ as a proxy of the boundary layer conditions. The *NuSTAR* flux was similar to that during the normal state as seen by BAT (2004 December 8 through 2010 October 13, and 2012 August 2 to 2016 January 11; see Figure 1 of Mukai et al. 2016). As the 2015 November *Swift* observations took place during the normal state, the instantaneous X-ray flux at that time was probably similar to the *NuSTAR* measurement; however, we cannot be certain due to the optical loading issue affecting the XRT data.

Therefore, $L_{\rm X;15-35keV}$ was formally constant (about $1.2\times10^{32}(d/640\,{\rm pc})^2\,{\rm erg\,s^{-1}}$) while $L_{\rm UV}$ dropped from $1.1\times10^{34}(d/640\,{\rm pc})^2\,{\rm erg\,s^{-1}}$ to $1.3\times10^{33}(d/640\,{\rm pc})^2\,{\rm erg\,s^{-1}}$, with $L_{\rm UV}/L_{\rm X;15-35keV}$ changing from 84 to 11. Even in a narrow band (2000–4000 Å), the UV luminosity exceeds the estimated bolometric X-ray luminosity (estimated to be $9.8\times10^{32}(d/640\,{\rm pc})^2\,{\rm erg\,s^{-1}}$), whereas in the case of an optically thin boundary layer, it is expected that X-ray emission roughly equals the bolometric disk luminosity. These UV and X-ray features suggest (i) a substantial decrease in the total mass accretion rate and (ii) that more of the boundary layer became optically thin to X-ray photons, so that any decrease in X-ray luminosity that we might have expected from the drop in accretion rate was compensated for by the increased fraction of the boundary layer emitting in the X-ray regime.

5. Summary

The main findings of this paper came from the first reliable X-ray spectroscopy of SU Lyn and complementary UV photometry. They are as follows:

1. The hard X-ray spectrum is consistent with the presence of reflection of hard X-rays from cold material, with reflection amplitude (R) equal to 1.
2. We revised the WD mass estimate from Mukai et al. (2016), taking into account the effects of the reflection component, with $R=1$ and $R=0$ fits resulting in a minimum mass between about 0.7 and $0.8\,M_{\odot}$, respectively.
3. We identified strong and variable intrinsic X-ray absorption, with rapid variability suggesting that the absorber is near the accreting white dwarf.
4. The X-ray absorber appears not to absorb UV. This implies that the absorber is extremely localized, predominantly in the line of sight of the primary X-ray emitter, and/or significantly ionized, and therefore without molecules and dust that could affect the UV photons.
5. Between 2015 November and 2016 August, the $L_{\rm UV}/L_{\rm X}$ ratio dropped dramatically, supporting a decrease in accretion rate while the boundary layer became more optically thin.

We encourage further observations of SU Lyn to refine our findings and to take further advantage of its long-term variability to study the response of accretion disk and the boundary layer to changes in accretion rate.

R.L.O. was partially supported by the Brazilian agency CNPq (PDE 200289/2017-9, Universal grants 459553/2014-3 and PQ 302037/2015-2). J.L.S. acknowledges support from NASA grants NNX15AF19G and NNX17AC45G. G.J.M.L. is a member of the CIC-CONICET (Argentina) and acknowledges support from grant ANPCYT-PICT 0478/14 and PIP-CONICET/2011 #D4598. The authors acknowledge Katja Pottschmidt and Brian Grefenstette for their guidance on reduction of *NuSTAR* data. This research has made use of the NuSTAR Data Analysis Software (NuSTARDAS), jointly developed by the ASI Science Data Center (ASDC, Italy) and the California Institute of Technology (Caltech, USA). This research has made use of the XRT Data Analysis Software (XRTDAS) developed under the responsibility of the ASI Science Data Center (ASDC), Italy. This work made use of data supplied by the UK Swift Science Data Centre at the University of Leicester. This research has made use of data, software and web tools obtained from the High Energy Astrophysics Science Archive Research Center (HEASARC), a service of the Astrophysics Science Division at NASA/GSFC and of the Smithsonian Astrophysical Observatory's High Energy Astrophysics Division. This work has made use of data from the European Space Agency (ESA) mission *Gaia* (https://www.cosmos.esa.int/gaia), processed by the *Gaia* Data Processing and Analysis Consortium (DPAC, https://www.cosmos.esa.int/web/gaia/dpac/consortium). Funding for the DPAC has been provided by national institutions, in particular the institutions participating in the *Gaia* Multilateral Agreement.

Facilities: *Swift* (XRT, BAT, and UVOT), *NuSTAR* (FPMA and FPMB).

ORCID iDs

R. Lopes de Oliveira https://orcid.org/0000-0002-6211-7226
J. L. Sokoloski https://orcid.org/0000-0003-2835-0304
G. J. M. Luna https://orcid.org/0000-0002-2647-4373
K. Mukai https://orcid.org/0000-0002-8286-8094
T. Nelson https://orcid.org/0000-0001-7009-2260

References

Anders, E., & Grevesse, N. 1989, GeCoA, 53, 197
Byckling, K., Mukai, K., Thorstensen, J. R., & Osborne, J. P. 2010, MNRAS, 408, 2298
Eze, R. N. C., Luna, G. J. M., & Smith, R. K. 2010, ApJ, 709, 816
Ezuka, H., & Ishida, M. 1999, ApJS, 120, 277

Frank, J., King, A., & Raine, D. J. 2002, Accretion Power in Astrophysics (3rd ed.; Cambridge: Cambridge Univ. Press), 398
Gaia Collaboration, Brown, A. G. A., Vallenari, A., et al. 2018, arXiv:1804.09365
Gaia Collaboration, Prusti, T., de Bruijne, J. H. J., et al. 2016, A&A, 595, A1
Gehrels, N., Chincarini, G., Giommi, P., et al. 2004, ApJ, 611, 1005
Harrison, F. A., Craig, W. W., Christensen, F. E., et al. 2013, ApJ, 770, 103
Horne, K., Marsh, T. R., Cheng, F. H., Hubeny, I., & Lanz, T. 1994, ApJ, 426, 294
Israel, G. L., & Stella, L. 1996, ApJ, 468, 369
Kenyon, S. J. 1986, The Symbiotic Stars (New York: Cambridge Univ. Press)
Luna, G. J. M., Mukai, K., Sokoloski, J. L., et al. 2018, arXiv:1801.02492
Luna, G. J. M., Sokoloski, J. L., Mukai, K., & Nelson, T. 2013, A&A, 559, A6
Madsen, K. K., Harrison, F. A., Markwardt, C. B., et al. 2015, ApJS, 220, 8
Magdziarz, P., & Zdziarski, A. A. 1995, MNRAS, 273, 837
Mukai, K. 2017, PASP, 129, 062001
Mukai, K., Luna, G. J. M., Cusumano, G., et al. 2016, MNRAS, 461, L1
Pringle, J. E., & Webbink, R. F. 1975, MNRAS, 172, 493
Vaughan, S. 2005, A&A, 431, 391
Wilms, J., Allen, A., & McCray, R. 2000, ApJ, 542, 914